# Modulating NLRP3 splicing with antisense oligonucleotides to control pathological inflammation

Roni Klein [1,2], Janset Onyuru [3], Estela M. Viera [1], Christopher D. Putnam [4], Hal M. Hoffman [3], Michelle L. Hastings [1,5]*

[1] Center for Genetic Diseases, Chicago Medical School, Rosalind Franklin University of Medicine and Science, North Chicago, Illinois, USA;
[2] School of Graduate and Postdoctoral Studies, Rosalind Franklin University of Medicine and Science, North Chicago, Illinois, USA;
[3] Department of Pediatrics, University of California San Diego, La Jolla, California, USA;
[4] Department of Medicine, University of California San Diego, La Jolla, California, USA;
[5] Department of Pharmacology, University of Michigan Medical School, Ann Arbor, Michigan, USA.

* To whom correspondence should be directed: hastingm@umich.edu

## Abstract

Inflammation has an essential role in healing. However, over-active inflammation disrupts normal cellular functions and can be life-threatening when not resolved. The NLRP3 inflammasome, a component of the innate immune system, is an intracellular multiprotein complex that senses stress-associated signals, and, for this reason is a promising therapeutic target for treating unresolved, pathogenic inflammation. Alternative splicing of *NLRP3* RNA has been suggested as a regulatory mechanism for inflammasome activation, as some spliced isoforms encode NLRP3 proteins with compromised function. Here, we take advantage of this natural regulatory mechanism and devise a way to control pathogenic inflammation using splice-switching antisense oligonucleotides (ASOs). To identify and induce NLRP3 spliced isoforms lacking inflammatory activity, we tested a series of ASOs, each targeting a different exon, to determine the most effective strategy for down-regulating NLRP3. We identify several ASOs that modulate *NLRP3* splicing, reduce NLRP3 protein, and decrease inflammasome signaling *in vitro*. The most effective ASO suppresses systemic inflammation *in vivo* in mouse models of acute inflammation and cryopyrin-associated periodic syndrome (CAPS). Our results demonstrate a systematic approach to protein engineering using splice-switching ASOs to generate isoforms with altered activity, and identify an ASO that can treat pathological inflammation in mice by reducing functional NLRP3.

## Introduction

The innate immune system defends against infectious and non-infectious threats, and inflammasomes are crucial mediators of this response. These intracellular multiprotein complexes detect microbial motifs and danger-associated molecules and mount an inflammatory response (1). Inflammasomes are categorized by their structural motifs. NLR-type inflammasomes have receptors with nucleotide-binding domain leucine-rich repeat (NLR) domains (2). The NLRP3 inflammasome (NLR family pyrin-containing protein 3) regulates the cellular response to pathogens and inflammatory insults that threaten cells. Once activated, NLRP3 forms an inflammasome complex that includes ASC (apoptosis-associated speck-like protein containing a CARD) and caspase 1 (CASP1), which self-cleaves and mediates interleukin-1β (IL-1β) and interleukin-18 (IL-18) maturation and secretion. Mature CASP1 also disinhibits gasdermin D (GSDMD), which leads to pore formation on the cell membrane and pyroptotic cell death, thereby eliminating infected or damaged cells (3). If not resolved, the pro-inflammatory cytokine cascade can alter normal cellular functions and further propagate an inflammatory response that can lead to tissue damage (4).

Although inflammation is a natural way for the body to respond to pathogens and eliminate damaged cells, endogenous stress signals can lead to aberrant NLRP3-mediated inflammation (5-8). Persistent NLRP3 inflammasome activation has been implicated in the pathogenesis of autoinflammatory, neurodegenerative, and metabolic diseases (9-11). Furthermore, gain of function mutations in *NLRP3* cause cryopyrin-associated periodic syndrome (CAPS), a rare pediatric autoinflammatory disease of varying severity resulting from dysregulation of the NLRP3 inflammasome and

uncontrolled release of inflammatory cytokines such as IL-β and IL-18 and pyroptosis (12, 13). In its most severe forms, Muckle-Wells syndrome (MWS) and neonatal-onset multisystem inflammatory disorder (NOMID), the disease presents with systemic, cutaneous, musculoskeletal, and central nervous system (CNS) inflammation, leading to progressive organ damage and dysfunction (14). Inhibition of inflammasome signaling has been a therapeutic goal in cases of chronic and pathogenic inflammation that becomes detrimental to life.

A number of approaches are being pursued in the clinic to therapeutically block the inflammasome; though, to date, there are still no good treatment options for many forms of NLRP3-mediated inflammation (3, 11). An alternative therapeutic approach is modulation of NLRP3 expression with antisense oligonucleotides. ASOs are short, synthetic, modified nucleic acids that base-pair to a target RNA and modulate its expression in a manner that depends on the specific ASO design. Splice-switching ASOs base-pair to pre-mRNA and alter splicing by blocking sequences that control splicing (15). In this way, they can be used as a therapeutic approach for modulating alternative splicing to increase or decrease mRNA transcripts encoding protein isoforms with differential activities. ASOs have many favorable drug-like qualities, including high target specificity, stability in cells and favorable safety profiles (16). Indeed, ASO medicines have had clinical success for a variety of conditions (15, 17).

To investigate the potential of splice-switching ASOs for NLRP3-associated pathogenic inflammation, we systematically evaluated the activity of NLRP3 isoforms induced by ASO-mediated splice-switching and identified ASOs that effectively suppress NLRP3-dependent activation in THP-1 cells and iBMDMs. Treatment with our

most effective ASO partially suppresses systemic inflammation in a mouse model of sepsis and prolongs survival in a murine model of CAPS, demonstrating that modulation of *NLRP3* with splice switching ASOs has therapeutic value in treating NLRP3-driven inflammatory diseases.

## Results

*Systematic ASO screening reveals induced NLRP3 spliced isoforms that suppress inflammasome activation.*

To identify the most effective approach to reducing NLRP3 activity using splice-switching ASOs, we targeted splicing of exons that either disrupt the protein open-reading frame when skipped (exon 2) or that encode critical structural features of the protein such as the linker (exon 3), or LRR domains (exon 5-9) (**Figure 1A**). ASOs that base-pair at the 3' or 5' splice sites (ss) were transfected into monocytic THP-1 cells that were differentiated into macrophage-like cells. Cells were primed with lipopolysaccharide (LPS) and subsequently activated with ATP to initiate the NLRP3 inflammatory response. RNA was isolated and splicing was analyzed by RT-PCR. ASO-Δ2 targeting exon 2 resulted in splicing from an alternative 5'ss in the upstream untranslated region of exon 2 to the 3'ss of exon 3, which splices out the natural start codon of the transcript. ASO-Δ3 activated an in-frame alternative 5'ss in the exon, resulting in partial deletion of the coding sequence. ASO-Δ5, Δ7 and Δ9 induced skipping of their respective exons. ASO-Δ6, targeting the 3'ss of the exon, activated an in-frame, cryptic 3'ss. ASO-Δ8 activated an out-of-frame 5'ss, resulting in partial exon 8 skipping and creation of a stop codon in exon 9 (**Figure 1A,B**). Some ASOs also induced a low level of additional splicing events. Overall, treatment of cells with ASOs

targeting exons 2, 3, 5, 6, 7, and 8, caused a significant decrease in full-length *NLRP3* mRNA compared to non-targeted, control ASO (ASO-C) (**Figure 1C**).

ASO-induced modulation of *NLRP3* exons 2, 5 and 8 splicing resulted in a significant decrease in NLRP3 protein abundance (**Figure 2A,B**). The ASO-induced exon skipping of other exons are expected to produce proteins with small in-frame deletions of the targeted exon coding sequence, which is not expected to reduce overall abundance of the protein.

To evaluate whether ASO-mediated exon skipping and consequent modulation of NLRP3 protein expression reduced the cellular inflammatory response, IL-1β release into the media was quantified following activation. ASO-Δ2, ASO-Δ6, and ASO-Δ8 significantly reduced IL-1β secretion from THP-1 cells in response to LPS and ATP (**Figure 2C**). As expected, there were no observed changes in the secreted levels of tumor necrosis factor-α (TNF-α), a proinflammatory cytokine produced by activated macrophages in response to independently of the NLRP3 pathway (**Figure 2D**). Protein modeling of NLRP3 ∆6 and ∆8 isoforms suggests that these deletions likely disrupt LRR-LRR interactions in the oligomerized form, likely explaining the reduced activity (**Supplemental Figure 1**). ASO-Δ2 skips the AUG codon in exon 2 and decreases NLRP3 protein expression due to the lack of methionine recognition by the ribosomal machinery.

Further testing of the most active ASOs, ASO-Δ2 and ASO-Δ6, identified their half-maximal inhibitory concentration (IC50) as 2.4 µM and 2.7 µM, respectively (**Figure 3A-E**). Treatment with these ASOs resulted in a dose-dependent decrease in IL-1β secretion (**Figure 3F**). The level of inhibition was similar to that observed in cells treated

with MCC950, a potent and specific small molecule inhibitor of NLRP3 (**Figure 3G**) (18). TNF-α levels were unaffected, suggesting that the ASOs are acting in an on-target manner specific to reducing NLRP3 activity without exerting an immunogenic effect (**Figure 3F**). To evaluate ASO-Δ2 in an *in vitro* model directly relevant to clinical, pathological NLRP3 activation, we introduced it into human monocyte-derived macrophages (hMDM) from individuals with CAPS harboring an *NLRP3* p.L353P mutation. Splicing analysis showed that ASO-Δ2 modulated *NLRP3* exon 2 skipping in hMDMs, confirming ASO activity in human primary cells (**Supplemental Figure 2**).

*ASO-mediated modulation of Nlrp3 splicing dampens inflammasome signaling in immortalized mouse macrophages.*

Next, we examined the therapeutic efficacy of mouse splice-switching ASOs on NLRP3 suppression in immortalized bone-marrow derived macrophages (iBMDMs). We tested ASOs that targeted the exon-intron junction of exon 2 (pyrin domain), 3 (linker domain), and 5-9 (LRR domains). ASOs effectively modulated alternative splicing of exon 2, 3, 5, 6, 8, and 9 but not exon 7 in iBMDMs treated with LPS and ATP. The respective ASOs induced skipping of exons 3, 5, 6, 8 and 9 and partial skipping of exon 2 (**Figure 4A-B**). ASOs targeting exons 2, 3, 6, and 8 also decreased full-length NLRP3 protein expression and cleavage of CASP1 (**Figure 4C-E**). IL-1β secretion was significantly reduced following treatment of cells with all ASOs except ASO-Δ5 and Δ7 (**Figure 4F**). Since inflammatory cell death occurs in iBMDMs in response to NLRP3 activation, we measured lactate dehydrogenase (LDH), a marker of pyroptosis, and found a significant decrease in levels following treatment all ASOs except ASO-Δ7,

which did not effectively target exon 7 (**Figure 4G**). LPS-dependent TNF-α levels in the media were unaffected by *Nlrp3*-targeted ASO activity (**Figure 4H**).

ASO-Δ2, the most active ASO, decreased full-length *Nlrp3* mRNA expression (IC50 of 32.4 µM) and IL-1β release in a dose-dependent manner (**Figure 5C-D**). Sanger sequencing revealed that ASO-Δ2 resulted in the activation of an alternative 5' splice site leading to an mRNA with a shifted open reading frame, creating a premature termination codon (PTC) in exon 3 (**Figure 5A-B**). ASO-Δ2 was selected for testing *in vivo* in mouse models of NLRP3-mediated inflammatory disease.

*Splice switching ASO suppresses systemic inflammation in an LPS model of sepsis.*

To examine the therapeutic potential of ASO-Δ2 *in vivo*, we tested its efficacy in a mouse model of acute infection that employs LPS, a potent pro-inflammatory endotoxin found in the outer membrane of gram-negative bacteria that activates innate immune signal and thereby mimics sepsis, a life-threatening sequela of infection. Previous studies have shown that peripheral LPS injection induces an NLRP3-dependent inflammatory response in mice (19). To ASO-Δ2 in this model, mice were treated with three doses of ASO-Δ2, ASO-C, or vehicle control by intraperitoneal (IP) injection on day 1, 3, and 6. On day 7, mice were injected with LPS or vehicle control and euthanized 3 hours later (**Figure 6A**). Analysis of plasma from the mice showed that treatment with ASO-Δ2 significantly reduced IL-1β and interleukin-6 (IL-6), a downstream pro-inflammatory cytokine, but not TNF in response to LPS induction compared to controls (**Figure 6B-D**). There were no significant differences between

vehicle control and non-targeted ASO-C. These results provide evidence for the anti-inflammatory activity of ASO-induced *Nlrp3* exon 2 skipping *in vivo*.

*ASO treatment prolongs survival and alleviates inflammation in a CAPS mouse model.*

To further assess the therapeutic efficacy of ASO-Δ2 in a clinically relevant model, we investigated its activity in a mouse model of CAPS. *Nlrp3*$^{D301N/+\ LysMCre+}$ mice express constitutively active NLRP3 protein in the myeloid lineage. This mutation in mouse *Nlrp3* corresponds to the human D303N mutation which causes NOMID, a severe form of CAPS (20). *Nlrp3* $^{D301N/+\ LysMCre+}$ mice develop severe multi-organ inflammation characterized by excessive secretion of proinflammatory cytokines, impaired growth, skin lesions, and perinatal death (20). *Nlrp3*$^{D301N/+\ LysMCre+}$ neonates were treated by subcutaneous (S.Q.) injection with ASO-Δ2 or vehicle control on postnatal (P) day 1, 3, and every 3 days thereafter until P24 or mouse death (**Figure 7A**). Treatment with ASO-Δ2 significantly prolonged survival (P=0.0003, Gehan-Breslow-Wilcoxon test), with 50% of mice surviving to P30 (maximum survival to P57) compared to controls, which survived to P15.5 (maximum survival to P20) (**Figure 7B**). Skin lesions on the abdomen and neck improved visually with ASO-Δ2 treatment and histopathological analysis revealed lower neutrophil infiltration in the skin compared to controls (**Figure 7C-E**). Body weight and spleen size were not significantly different between ASO-treated and control groups (**Supplemental Figure 3**). ASO-Δ2-treated mice exhibited decreased levels of IL-1β and IL-18 but not IL-6 or TNF in the serum compared to controls at P12, demonstrating that ASO-induced *Nlrp3* exon 2 skipping has a systemic anti-inflammatory NLRP3 dependent effect in response to CAPS mutation associated constitutive NLRP3 activation (**Figure 7F-I**). These data show that

ASO-mediated modulation of *Nlrp3* exon 2 splicing ameliorates the clinical phenotype of CAPS in mice.

## Discussion

Inflammation is increasingly recognized as a contributing factor to the development of serious, often chronic diseases and cancers, representing an area of unmet therapeutic need. The NLRP3 inflammasome contributes to pathological inflammation in numerous conditions. Direct NLRP3 inhibition is a means to short-circuit the inflammatory response early in the activation pathway to specifically control aberrant NLRP3-associated inflammation and lessen disease severity. Here, we demonstrate that splice-switching ASOs provide a specific and effective therapeutic strategy for suppressing NLRP3-mediated inflammatory signaling. These ASOs induce splicing alterations that result in mRNAs encoding non-functional NLRP3 protein isoforms that are unstable and/or lack functional domains essential for inflammasome assembly and activation.

One of the most effective ASOs at modulating splicing and down-regulating NLRP3 activity modulates exon 2 splicing in THP-1 cells. The human *NLRP3* exon 2-targeted ASO blocks splicing at the dominant exon 2 5’ splice site (ss) and activates splicing at an alternative 5’ss in the exon, upstream of the start codon. Splicing at this upstream 5’ss to the natural 3’ss of exon 3, results in splicing out of the AUG start codon in exon 2, thereby decreasing NLRP3 protein expression due to the lack of its translation initiation site. Notably, ASO-Δ2 modulates *NLRP3* exon 2 skipping in hMDMs from CAPS patients (**Supplemental Figure 2**), confirming ASO activity in human

primary cells and offering promise for ASO-mediated exon skipping effectiveness in mitigating inflammasome signaling in disease-relevant cells.

Blocking exons 6 or 8 splicing with ASOs also results in impaired inflammasome signaling. ASO-Δ6 activates an in-frame alternative 3' ss resulting in deletion of a small segment of the LRR domain (774-794 aa) and introduction of a single nucleotide polymorphism at position S795C. ASO-Δ8 activates a cryptic 5'ss in exon 8 resulting in a shifted reading frame and creation of a PTC in exon 9, making the transcript susceptible to nonsense-mediated mRNA decay (NMD). The functional impact that we observe experimentally by inducing an internal deletion and protein truncation with ASO-Δ6 and Δ8, respectively, is supported by structural analysis of the protein isoforms as well. Recent cryo–electron microscopy (cryo-EM) studies suggest that NLRP3 forms an oligomer consisting of 10 subunits, creating a double cage-like structure (**Supplemental Figure 1**). Neighboring LRR domains from the two discs interact with each other front and back (21, 22). Our protein modeling of NLRP3 isoforms indicates that the Δ6 isoform lacks a region of the LRR involved in the convex interaction and that the Δ8 isoform deletes most of the regions making up the concave interactions. We predict that both isoforms, but particularly the Δ8 isoform, disrupt the stability of the decameric cage. The Δ6 isoform could both weaken the convex interactions as well as alter the concave interactions by changing the spacing of the LRR repeats C-terminal to the deletion. Importantly, a single ASO-induced NLRP3 isoform monomer can potentially destabilize an oligomerized structure formed with full-length NLRP3, thereby exerting a dominant negative effect that could amplify the effect of the ASO treatment. The LRR deletion in NLRP3 Δ6 is unlikely to affect the formation of the decameric disk,

as these interactions are mediated by the FIS and NACHT domains that are not predicted to be affected in the Δ6 and Δ8 isoform structure. In contrast, the Δ8 isoform lacks many of the amino acids involved in the full-length LRR-NEK7 interaction, which predicts a weakened interaction (**Supplemental Figure 1**).

In mouse iBMDMs, ASO-Δ6 and Δ8 induce skipping of the entire targeted exon, which results in attenuation of inflammasome activation. The effect is likely due to deletions of segments of the LRR domain. Mouse NLRP3 subunits also form a dodecamer with interacting LRR domains to support complex stability (23). Our results suggest that ASO-mediated deletions of LRR segments may destabilize the 12-subunit structure, offering an explanation as to how these isoforms are less active.

ASO-mediated *Nlrp3* partial exon 2 skipping results in a premature termination codon (PTC) that is predicted to make a small peptide (78 aa). The PTC also makes the transcript susceptible to nonsense-mediated mRNA decay (NMD) (**Figure 5**). The therapeutic potential of using ASO-Δ2 to treat systemic inflammation and alleviate disease severity is supported by our results demonstrating efficacy in mouse models of pathological inflammation. Administration of ASO-Δ2 partially suppresses IL-1β and IL-6 levels in the plasma in response to peripheral LPS challenge, providing evidence for a protective effect against NLRP3 activation. Treatment with ASO-Δ2 also prolonged survival and decreased systemic inflammation in a mouse model of cryopyrin-associated periodic syndrome (CAPS) expressing a missense mutation in *Nlrp3* (D301N). ASO-Δ2-treated mice exhibited decreased IL-1β and IL-18 levels in the serum compared to control mice treated with vehicle only, suggesting that ASO-mediated NLRP3 inhibition protects against constitutive inflammasome activation *in vivo*. Notably,

improved skin lesions, return of hair follicles, and reduction in neutrophil infiltration in the skin reveal the potential efficacy of ASO-based approaches in addressing other inflammatory skin diseases. Overall, we show that ASO-mediated reduction in functional NLRP3 inflammasome signaling can therapeutically reduce disease-severity in mouse models of inflammation.

Other ASO-based strategies have been investigated as a means to reduce NLRP3. Specifically, an RNase H-targeting Nlrp3 ASO (gapmer), which results in degradation of the RNA, was shown to lower *Nlrp3* expression and extend the life of mice modeled to have CAPS (24). These results further support ASO approaches for modulating NLRP3 activity. Both splice-switching and RNase H-targeting ASOs have had clinical success in treating disease, making them promising candidate platforms for treating NLRP3-associated conditions (25-28).

ASOs have had clinical success in disorders of the central nervous system, particularly because they can be safely administered by intrathecal injection for direct and efficient targeting. Thus, the therapeutic utility of *NLRP3*-targeted ASOs can be extended to neurological disorders that have been associated with the inflammasome. For example, in Alzheimer's disease (AD), Aβ deposition triggers NLRP3 inflammasome activation in glial cells (7, 29). Human studies reveal elevated ASC specks and mature Casp1 in the prefrontal cortex and hippocampus of AD brains compared to control brains postmortem (7). Notably, reducing *Nlrp3* by genetic knockout or using small molecule NLRP3 inhibitors has shown efficacy in reducing neuroinflammation and ameliorating AD symptoms in mouse models (7, 30, 31). These results provide

evidence of the potential utility of *NLRP3*-targeted ASOs for mitigating neuroinflammation associated with neurodegenerative diseases.

ASOs offer an alternative to current treatment approaches and therapeutic strategies for targeting the NLRP3 inflammasome. To date, there are three IL-1 blockers approved by the FDA and EMA (11). However, because IL-1β is an important signaling component of other inflammasomes, not only the NLRP3 inflammasome, IL-1 inhibition compromises the innate immune system in a more global manner, thereby posing a high risk for infections and other potentially dangerous side-effects (32). NLRP3-specific inhibitors offer a more specific approach to treating pathogenic inflammation mediated by the NLRP3 inflammasome and can also address other effects of NLRP3 activation, such as IL-18 secretion and pyroptosis, which contribute to lingering inflammation in IL-1β knockout CAPS mice (33). Recent studies have reported on small molecule inhibitors that target NLRP3 and alleviate inflammation associated with CAPS and other conditions (3, 18, 34, 35). These NLRP3 inhibitors are more effective than IL-1β inhibitors in mouse models of CAPS, suggesting that inactivating the inflammasome directly will provide greater therapeutic value than targeting downstream released cytokines. Though promising results have been reported with NLRP3 inhibitors for a number of conditions, toxicities and off-target effects have been a concern in some cases and small molecule NLRP3 inhibitors are less effective for CAPS-associated mutations that disrupt the binding pocket of such compounds (36, 37). Hence, manipulating NLRP3 gene expression directly using ASOs is an attractive alternative approach for treating NLRP3-driven inflammation.

This study demonstrates a systematic approach for identifying potentially therapeutic splice-switching ASOs and specifically demonstrates the therapeutic potential of targeting *NLRP3* splicing with ASOs to control pathogenic inflammation. The identified ASOs offer a potentially therapeutic alternative to approved IL-1β drugs or small molecule NLRP3 inhibitors currently in clinical trials. The growing success of ASO drugs in the clinic and in clinical trials, supports the promise of an *NLRP3*-targeted ASO as a safe, durable, and highly specific therapeutic for treating NLRP3-mediated inflammatory disease.

## Methods

*Sex as a biological variable*

Our study examined females in the LPS challenge because they exhibited a greater immune response compared to male mice in pilot studies. However, the findings could apply to males and females because NLRP3 is expressed in both sexes. Our CAPS model examined male and female animals, and no significant differences due to sex were observed in the *in vivo* ASO treatment of neonates.

*Antisense oligonucleotides and nomenclature*

Splice switching antisense oligonucleotides are phosphorodiamidate morpholinos (PMO) (Gene Tools, LLC) (**Supplemental Table 1**). A non-targeting PMO was used as a negative control (Gene Tools, standard control oligo). BLAST analysis of human ASO-Δ2 found no off-target complementary sequences of greater than 15 contiguous nucleotides. Lyophilized ASOs were formulated in filtered deionized $H_2O$, 0.9% saline,

or Dulbecco's phosphate-buffered saline (DPBS). The identity of ASO-induced *NLRP3* isoforms was determined by Sanger sequencing.

*Cell culture and transfections*

THP-1 (ATCC TIB-202), a monocytic cell line isolated from peripheral blood from an acute monocytic leukemia patient, was cultured in Roswell Park Memorial Institute (RPMI) 1640 supplemented with 10% fetal bovine serum (FBS) and 0.05 mM 2-Mercaptoethanol (BME) at 37 °C and 5% carbon dioxide ($CO_2$). THP-1 cells were seeded at $5x10^5$ cells/mL, differentiated with 50 ng/mL phorbol 12-myristate 13-acetate (PMA) for 24 hours, and transfected 18 hours later (38, 39). Immortalized murine bone-marrow derived macrophages (iBMDMs) (a gift from Dr. Venkat Magupalli and Dr. Hao Wu) were cultivated in Dulbecco's Modified Eagle's medium (DMEM) supplemented with 10% FBS at 37 °C and 5% $CO_2$. iBMDMs were plated at 40-50% confluency and incubated for 18 hours. ASOs with a PMO chemistry were transfected into THP-1 and iBMDM at a final concentration of 40 µM using Endo-Porter (Gene Tools, LLC) for 48 hours according to manufacturer instructions (Gene Tools, LLC). Human monocyte-derived macrophages (hMDM) from CAPS patients harboring a L353P mutation in *NLRP3* were differentiated with 20 ng/mL macrophage colony-stimulating factor (M-CSF) for 7 days. On day six, ASO-Δ2 was transfected with Endo-Porter (Gene Tools LLC) into the cells at a final concentration of 40 µM for 24 hours. The lysate was collected for splicing analysis.

*Inflammasome activation assay*

PMA-differentiated THP-1 cells and iBMDMs were transfected with ASOs as described above and incubated for 48 hours. Cells were then primed with 100 ng/mL LPS (*Escherichia coli* 055:B5, Sigma) in supplemented media for 3 hours. Subsequently, media was removed and cells were activated with 5 mM ATP (Invivogen) in OptiMem (Thermo Fisher) for 1 hour. MCC950 (Invivogen) was added in OptiMem (Thermo Fisher) 30 minutes prior to activation with 5 mM ATP for 1 hour. Media was collected for analysis of released signaling molecules and lysate was collected for RNA and protein analysis.

*RNA isolation and analysis*

Total RNA was extracted from cells or mouse tissue using TRIzol according to the manufacturer's instructions (Thermo Fisher). RNA (1μg) was reverse transcribed using GoScript reverse transcriptase (Promega) and oligo-dT primer. Radiolabeled RT-PCR of cDNA was performed using GoTaq Green (Promega) with alpha-$^{32}$P-deoxycytidine triphosphate (dCTP), and primers for NLRP3 (**Supplemental Table 1, Figures 1,4**). PCR products were resolved on a 6% non-denaturing polyacrylamide gel and quantified using a Typhoon FLA 7000 phosphorimager (GE Healthcare). The percent of the NLRP3 mRNA including the targeted exon was calculated relative to the abundance of the predominant ASO-induced isoform after the signal was corrected for the number of cytosine nucleotides. Predominant ASO-induced isoforms were isolated from agarose gel, column purified (Cytiva), and Sanger sequenced with NLRP3 primers (**Supplemental Table 1**).

*Real-time quantitative PCR*

Real-time qPCR was performed with PrimeTime Gene Expression Master Mix (Integrated DNA Technologies, IDT) and pre-designed NLRP3 (Thermo Fisher, Mm04210225_m1) and GAPDH (Thermo Fisher, Mm99999915_g1) probes. PCR was performed on an Applied Biosystems (ABI) ViiA 7 Real-Time PCR System with the following thermal-cycling protocol: stage 1–50°C for 2 min, 95°C for 3 min; stage 2 – 40 cycles of 95°C for 15 s, 60°C for 1 min. The relative quantity was calculated as $2^{-(\Delta\Delta Ct)}$ and multiplied by % FL, which is equal to FL/(FL+$\Delta$2), the abundance of full-length *Nlrp3* relative to sum of full-length and ASO-induced isoform.

*Immunoblot analysis*

Cells were lysed in RIPA buffer (150 mM NaCl, 50 mM Tris-Cl pH 7.6, 1% NP-40, 0.5% Na-DOC, 0.1% SDS) containing protease and phosphatase inhibitor cocktail (Thermo Fisher). Lysates were centrifuged at 10,000 x g for 20 min at 4 °C and protein concentration was determined by Bradford or Pierce BCA protein assay (Thermo Fisher). Supernatant was centrifuged using 10 kDa Amicon Ultra Centrifugal Filters (Millipore). Lysates and supernatants were prepared with 4x Bolt lithium dodecyl sulfate (LDS) and 10x dithiothreitol (DTT) and boiled in 95 °C for 5 minutes. Cell lysates were separated by 4–15% SDS-polyacrylamide electrophoresis (PAGE) tris-glycine precast gels (Bio-Rad) and supernatants were separated by 12% SDS-PAGE tris-glycine gels and both were transferred to a 0.45 $\mu$m immobilon-FL polyvinylidene difluoride (PVDF) blotting membrane (Millipore) at 75V for 1 hour. Membranes were blocked with 5% nonfat dry milk (NFDM) in Tris-buffered saline (TBS) supplemented with 0.1% Tween 20

(TBST) and probed with primary antibodies overnight at 4 °C using rabbit NLRP3 (1:1000, D4D8T-15101, Cell Signaling), mouse caspase 1 (1:1000, Casper 1- AG-20B-0042, Adipogen). Rabbit α-tubulin (1:1000, 11224-1-AP, Proteintech) was incubated with membrane for 1 hr at room temperature. Horseradish peroxidase (HRP)-conjugated rabbit and mouse secondary antibodies (Thermo Fisher, 1:5,000-1:20,000) were incubated with membrane for 1 hour at room temperature. Immunoblots were developed using Classico (Immobilon) or SuperSignal West Femto (Thermo Fisher) substrate and exposed to film. Western blot bands were quantified using ImageJ software.

*ELISA and LDH assay*

Supernatant, serum, plasma, and tissue were analyzed for IL-1β (human DY200, mouse DY401), IL-6 (mouse DY406), IL-18 (mouse DY7625), and TNF-α (human DY210, mouse DY410) by ELISA (R&D Systems) according to manufacturer's instructions. Optical density (450 nm – 540 nm) values are normalized to LPS- and ATP-stimulated cells and utilized to extrapolate the concentration from a standard curve *in vivo*. LDH release was measured with a CytoTox 96® Non-Radioactive Cytotoxicity Assay (G1780, Promega) and the percent of LDH was calculated relative to LPS and ATP stimulated cells.

*Mice*

Mice were maintained at 23 °C with a 12 h light/dark cycle with food and water available *ad libitum*. Wild-type C57BL/6 mice were purchased from The Jackson Laboratory and

bred at RFUMS. Mice bearing an aspartate 301 to asparagine (D301N) substitution were generated as previously described (The Jackson Laboratory: B6N.129-Nlrp3D301NneoR/J, strain no. 017971) (20, 40). The D301N point mutation leads to a conformational change causing a ligand-independent constitutive activation of the mutant *Nlrp3* inflammasome. Due to the presence of an intronic-floxed neomycin resistance cassette, *Nlrp3* gene expression is abolished. Expression of the mutant allele only occurs when the *Nlrp3* knock-in mice are bred with mice expressing Cre recombinase. *Nlrp3* knock-in mice were bred with mice expressing Cre recombinase under the control of lysozyme (CreL; The Jackson Laboratory, strain no. 004781, B6.129P2- Lyz2tm1(cre)Ifo/J), resulting in constitutive activation of mutant *Nlrp3* in the myeloid lineage.

*LPS challenge*

C57BL/6 female mice (7-8 weeks old) were intraperitoneally (I.P.) injected with ASO-Δ2 (100 mg/kg), ASO-C (100 mg/kg), or PBS on day 1,3, and 6. On day 7, mice were I.P. injected with 20 mg/kg ultrapure LPS from E. coli 0111:B4 (Invivogen, tlrl-3pelps) or PBS. Three hours later, the treated mice were euthanized, blood was collected in EDTA-coated syringes through cardiac puncture and diluted 1:1 in PBS. Diluted blood was added to Ficoll and centrifuged at 400 x g for 30 minutes. Plasma was collected and stored in -80 °C until analysis.

*CAPS mice*

*Nlrp3*$^{D301N/+\ LysMCre+}$ mice were injected with ASO-Δ2 (100 mg/kg) or PBS by subcutaneous injection on P1, P3 and then every 3 days until P24. Mice were monitored daily for growth and survival. Some mice were euthanized at P12 and tissue was collected, snap frozen in liquid nitrogen, and stored in -80 °C until further analysis.

*Histological staining analysis*

Mouse skin lesions from the nape were collected following euthanization. Hair around the lesion was removed using hair removal cream (Nair) with a gauze-tipped applicator. After 24 hours of fixation in 10% Buffered Formalin, the paraffin-embedded skin lesions were stained with hematoxylin and eosin (H&E). The slides were then reviewed by a blinded pathologist to identify derm layers and neutrophil infiltration. Scans of all sections were taken using a NanoZoomer 2.0HT Slide Scanning System (Hamamatsu Photonics, Hamamatsu, Japan). The number of neutrophils per section were quantified using a cell classifier on Qupath v0.5.1.

*Structure modeling*

Models of the human NLRP3 Δ6 and Δ8 isoforms were initially generated from the predicted protein sequences by Alphafold2 (41). The folds of the individual domains of the resulting models matched that of the experimental NLRP3 structures; however, the resulting conformation did not precisely match that of the known active or inactive conformations (22, 42), which are related by a rigid body motion between the FISNA-NBD-HD1 N-terminal subdomains of the NACHT domain and the WH-HD2-LRR domains (11). To build models of the Δ6 and Δ8 isoforms in the known active and

inactive conformations, the Alphafold2-predicted Δ6 and Δ8 leucine-rich repeats were superimposed onto the LRR repeats of the full-length active conformation (PDB id 8ej4) (42) and the full-length inactive conformation (PDB id 7pzc) (22). This analysis was performed by first calculating the affine transformation matrices to superimpose residues 651-683 of the Alphafold2 models onto residues 651-683 for each of the NLRP3 monomers in the inactive and active assemblies; this residue range includes NLRP3 regions involved in the WH-HD2-LRR rigid body motion but avoids residues deleted in the Δ6 and Δ8 isoforms. The affine transformations were then applied to the entire Alphafold2 modeled Δ6 and Δ8 LRR domains (residues 651-1034) and the transformed LRR domains were merged with residues 1-650 of the experimental structures.

*Statistical analysis*

All data were analyzed GraphPad Prism (version 10.2.3) and presented as the mean ±SEM (*P<0.05, **P<0.01, ***P<0.001, ****P<0.0001). For comparison of two groups, we utilized a two-tailed Student's t-test. Following a normality test, in cases of non-Gaussian distribution, we utilized a Mann-Whitney test. For more than 2 groups, we utilized one way ANOVA followed by post-hoc analysis as detailed in figure legends. ASO potency was calculated using the half maximal inhibitory concentration (IC50) after plotting the data on a nonlinear regression curve with a standard slope. Survival curve comparison was analyzed by Gehan-Breslow-Wilcoxon test. The specific statistical test used for each experiment is specified in the figure legends.

*Study approval*

All protocols met ethical standards for animal experimentation and were approved by the Institutional Animal Care and Use Committee of Rosalind Franklin University of Medicine and Science and University of California San Diego. Studies performed using PBMCs obtained from CAPS patients received the approval of the University of California Human Research Protection Program committee, and informed consent was obtained from the subjects before the study.

*Data availability*

Values for all data points in graphs are reported in the Supporting Data Values file. Uncropped radioactive RT-PCR gel scans and western blots are provided in a supplemental file. Any other data can be requested from the corresponding author.

## Author contributions

RK and MLH conceived and designed the study. RK, JO, and EMV conducted the experiments. RK, JO and MLH analyzed the data. CDP performed protein modeling. RK and MLH wrote the original draft of the manuscript. RK, JO, EMV, CDP, HMH, and MLH reviewed and edited the manuscript. HMH and MLH acquired funding and resources and supervised the project.

## Acknowledgments

The authors thank the patients for providing blood samples for this study. The authors thank Drs. Venkat Magupalli and Hao Wu for the iBMDM cells and Dr. Reid Oldenburg for histopathological assessments.

This work has been funded by NIH RO1 AG060195 and University discretionary funds to MLH and NIH RO1 AI15586901 to HMH. The proteomics facility at RFUMS was supported by NIH S10 OD010662.

Conflicts of interest: MLH has consulted with ProMIS Neurosciences and QurAlis and has had research collaborations with Ionis Pharmaceuticals; HMH has consulted for Novartis, Sobi, Ventyx, and Akros and has had research collaborations with Jecure, Zomagen, Takeda, and Inapill.

## References

1. Barnett KC, Li S, Liang K, and Ting JP. A 360 degrees view of the inflammasome: Mechanisms of activation, cell death, and diseases. *Cell.* 2023;186(11):2288-312.
2. Chou WC, Jha S, Linhoff MW, and Ting JP. The NLR gene family: from discovery to present day. *Nat Rev Immunol.* 2023;23(10):635-54.
3. Coll RC, Schroder K, and Pelegrin P. NLRP3 and pyroptosis blockers for treating inflammatory diseases. *Trends Pharmacol Sci.* 2022;43(8):653-68.
4. Meizlish ML, Franklin RA, Zhou X, and Medzhitov R. Tissue Homeostasis and Inflammation. *Annu Rev Immunol.* 2021;39:557-81.
5. Martinon F, Petrilli V, Mayor A, Tardivel A, and Tschopp J. Gout-associated uric acid crystals activate the NALP3 inflammasome. *Nature.* 2006;440(7081):237-41.
6. Duewell P, Kono H, Rayner KJ, Sirois CM, Vladimer G, Bauernfeind FG, et al. NLRP3 inflammasomes are required for atherogenesis and activated by cholesterol crystals. *Nature.* 2010;464(7293):1357-61.
7. Heneka MT, Kummer MP, Stutz A, Delekate A, Schwartz S, Vieira-Saecker A, et al. NLRP3 is activated in Alzheimer's disease and contributes to pathology in APP/PS1 mice. *Nature.* 2013;493(7434):674-8.

8. Trudler D, Nazor KL, Eisele YS, Grabauskas T, Dolatabadi N, Parker J, et al. Soluble alpha-synuclein-antibody complexes activate the NLRP3 inflammasome in hiPSC-derived microglia. *Proc Natl Acad Sci U S A.* 2021;118(15).
9. Toldo S, and Abbate A. The role of the NLRP3 inflammasome and pyroptosis in cardiovascular diseases. *Nat Rev Cardiol.* 2024;21(4):219-37.
10. Ravichandran KA, and Heneka MT. Inflammasomes in neurological disorders - mechanisms and therapeutic potential. *Nat Rev Neurol.* 2024;20(2):67-83.
11. Putnam CD, Broderick L, and Hoffman HM. The discovery of NLRP3 and its function in cryopyrin-associated periodic syndromes and innate immunity. *Immunol Rev.* 2024;322(1):259-82.
12. Hoffman HM, Mueller JL, Broide DH, Wanderer AA, and Kolodner RD. Mutation of a new gene encoding a putative pyrin-like protein causes familial cold autoinflammatory syndrome and Muckle-Wells syndrome. *Nat Genet.* 2001;29(3):301-5.
13. Agostini L, Martinon F, Burns K, McDermott MF, Hawkins PN, and Tschopp J. NALP3 forms an IL-1beta-processing inflammasome with increased activity in Muckle-Wells autoinflammatory disorder. *Immunity.* 2004;20(3):319-25.
14. Romano M, Arici ZS, Piskin D, Alehashemi S, Aletaha D, Barron KS, et al. The 2021 EULAR/American College of Rheumatology points to consider for diagnosis, management and monitoring of the interleukin-1 mediated autoinflammatory diseases: cryopyrin-associated periodic syndromes, tumour necrosis factor receptor-associated periodic syndrome, mevalonate kinase deficiency, and deficiency of the interleukin-1 receptor antagonist. *Ann Rheum Dis.* 2022;81(7):907-21.
15. Havens MA, and Hastings ML. Splice-switching antisense oligonucleotides as therapeutic drugs. *Nucleic Acids Res.* 2016;44(14):6549-63.
16. Hall J. Future directions for medicinal chemistry in the field of oligonucleotide therapeutics. *RNA.* 2023;29(4):423-33.
17. Collotta D, Bertocchi I, Chiapello E, and Collino M. Antisense oligonucleotides: a novel Frontier in pharmacological strategy. *Front Pharmacol.* 2023;14:1304342.
18. Coll RC, Robertson AA, Chae JJ, Higgins SC, Munoz-Planillo R, Inserra MC, et al. A small-molecule inhibitor of the NLRP3 inflammasome for the treatment of inflammatory diseases. *Nat Med.* 2015;21(3):248-55.
19. He Y, Franchi L, and Nunez G. TLR agonists stimulate Nlrp3-dependent IL-1beta production independently of the purinergic P2X7 receptor in dendritic cells and in vivo. *J Immunol.* 2013;190(1):334-9.
20. Bonar SL, Brydges SD, Mueller JL, McGeough MD, Pena C, Chen D, et al. Constitutively activated NLRP3 inflammasome causes inflammation and abnormal skeletal development in mice. *PLoS One.* 2012;7(4):e35979.
21. Fu J, and Wu H. Structural Mechanisms of NLRP3 Inflammasome Assembly and Activation. *Annu Rev Immunol.* 2023;41:301-16.
22. Hochheiser IV, Pilsl M, Hagelueken G, Moecking J, Marleaux M, Brinkschulte R, et al. Structure of the NLRP3 decamer bound to the cytokine release inhibitor CRID3. *Nature.* 2022;604(7904):184-9.

23. Andreeva L, David L, Rawson S, Shen C, Pasricha T, Pelegrin P, et al. NLRP3 cages revealed by full-length mouse NLRP3 structure control pathway activation. *Cell.* 2021;184(26):6299-312 e22.
24. Kaufmann B, de Los Reyes Jimenez M, Booshehri LM, Onyuru J, Leszczynska A, Uri A, et al. Antisense Oligonucleotide Therapy Decreases IL-1beta Expression and Prolongs Survival in Mutant Nlrp3 Mice. *J Immunol.* 2023;211(2):287-94.
25. Egli M, and Manoharan M. Chemistry, structure and function of approved oligonucleotide therapeutics. *Nucleic Acids Res.* 2023;51(6):2529-73.
26. Sheng L, Rigo F, Bennett CF, Krainer AR, and Hua Y. Comparison of the efficacy of MOE and PMO modifications of systemic antisense oligonucleotides in a severe SMA mouse model. *Nucleic Acids Res.* 2020;48(6):2853-65.
27. Takakusa H, Iwazaki N, Nishikawa M, Yoshida T, Obika S, and Inoue T. Drug Metabolism and Pharmacokinetics of Antisense Oligonucleotide Therapeutics: Typical Profiles, Evaluation Approaches, and Points to Consider Compared with Small Molecule Drugs. *Nucleic Acid Ther.* 2023;33(2):83-94.
28. Bennett CF, Baker BF, Pham N, Swayze E, and Geary RS. Pharmacology of Antisense Drugs. *Annu Rev Pharmacol Toxicol.* 2017;57:81-105.
29. Zhang L, Qian Y, Li J, Zhou X, Xu H, Yan J, et al. BAD-mediated neuronal apoptosis and neuroinflammation contribute to Alzheimer's disease pathology. *iScience.* 2021;24(9):102942.
30. Dempsey C, Rubio Araiz A, Bryson KJ, Finucane O, Larkin C, Mills EL, et al. Inhibiting the NLRP3 inflammasome with MCC950 promotes non-phlogistic clearance of amyloid-beta and cognitive function in APP/PS1 mice. *Brain Behav Immun.* 2017;61:306-16.
31. Lonnemann N, Hosseini S, Marchetti C, Skouras DB, Stefanoni D, D'Alessandro A, et al. The NLRP3 inflammasome inhibitor OLT1177 rescues cognitive impairment in a mouse model of Alzheimer's disease. *Proc Natl Acad Sci U S A.* 2020;117(50):32145-54.
32. Ridker PM, Everett BM, Thuren T, MacFadyen JG, Chang WH, Ballantyne C, et al. Antiinflammatory Therapy with Canakinumab for Atherosclerotic Disease. *N Engl J Med.* 2017;377(12):1119-31.
33. McGeough MD, Wree A, Inzaugarat ME, Haimovich A, Johnson CD, Pena CA, et al. TNF regulates transcription of NLRP3 inflammasome components and inflammatory molecules in cryopyrinopathies. *J Clin Invest.* 2017;127(12):4488-97.
34. Ma JH, Lee E, Yoon SH, Min H, Oh JH, Hwang I, et al. Therapeutic effect of NLRP3 inhibition on hearing loss induced by systemic inflammation in a CAPS-associated mouse model. *EBioMedicine.* 2022;82:104184.
35. Marchetti C, Swartzwelter B, Gamboni F, Neff CP, Richter K, Azam T, et al. OLT1177, a beta-sulfonyl nitrile compound, safe in humans, inhibits the NLRP3 inflammasome and reverses the metabolic cost of inflammation. *Proc Natl Acad Sci U S A.* 2018;115(7):E1530-E9.
36. Vande Walle L, Stowe IB, Sacha P, Lee BL, Demon D, Fossoul A, et al. MCC950/CRID3 potently targets the NACHT domain of wild-type NLRP3 but not

disease-associated mutants for inflammasome inhibition. *PLoS Biol.* 2019;17(9):e3000354.

37. Chen X, Zhang P, Zhang Y, Wei M, Tian T, Zhu D, et al. The research progression of direct NLRP3 inhibitors to treat inflammatory disorders. *Cell Immunol.* 2024;397-398:104810.

38. Tsuchiya S, Yamabe M, Yamaguchi Y, Kobayashi Y, Konno T, and Tada K. Establishment and characterization of a human acute monocytic leukemia cell line (THP-1). *Int J Cancer.* 1980;26(2):171-6.

39. Auwerx J. The human leukemia cell line, THP-1: a multifacetted model for the study of monocyte-macrophage differentiation. *Experientia.* 1991;47(1):22-31.

40. Hoffman HM. Autoinflammatory disease: New mouse models and therapies. *J Allergy Clin Immunol.* 2020;145(1):116-8.

41. Jumper J, Evans R, Pritzel A, Green T, Figurnov M, Ronneberger O, et al. Highly accurate protein structure prediction with AlphaFold. *Nature.* 2021;596(7873):583-9.

42. Xiao L, Magupalli VG, and Wu H. Cryo-EM structures of the active NLRP3 inflammasome disc. *Nature.* 2023;613(7944):595-600.

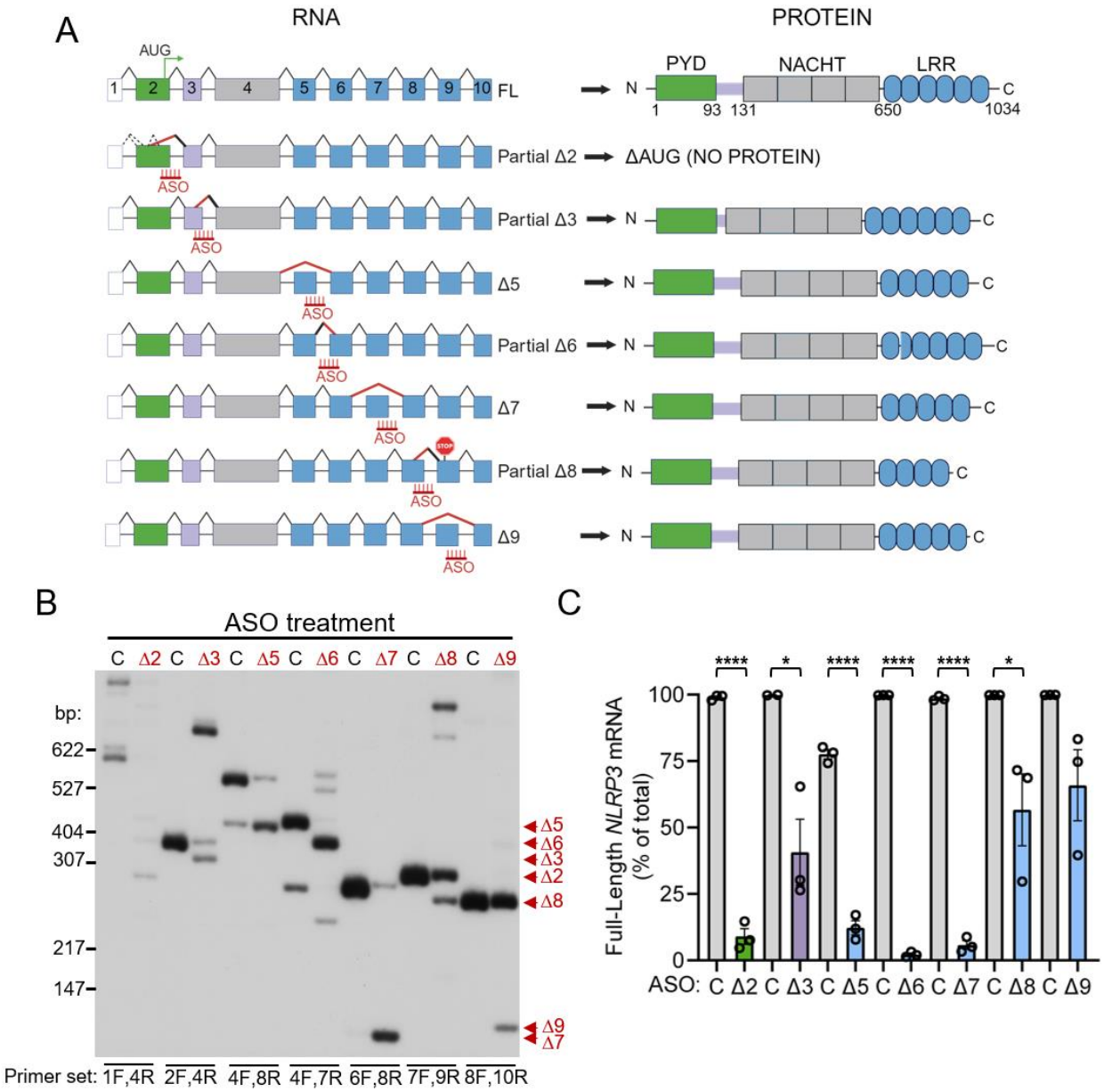


**Figure 1. *NLRP3*-targeted splice-switching ASOs modulate alternative splicing.**
**A)** Schematic of the predominant ASO-mediated *NLRP3* splice variants and predicted protein products translated from the induced spliced isoforms. (left) Boxes are exons and lines are introns. General ASO binding site is labeled. Diagonal black lines show splicing of introns. Dashed diagonal lines represent natural alternative splicing. Red diagonal lines indicate ASO-induced splicing event. (right) NLRP3 protein domains for full-length and corresponding translated spliced isoforms are shown. **(B)** Representative radioactive RT-PCR analysis of *NLRP3* RNA from THP-1 cells treated with indicated ASOs. Products were amplified using different primer sets for each ASO (see bottom of gel image) and separated by PAGE. Each pair of lanes (non-targeted ASO control (C) and a targeting ASO (ΔX)) shows different-sized products of the full-length and ASO-induced splice variant for each indicated ASO. Red arrowheads indicate predominant ASO-induced spliced isoform for each ASO. Some ASOs also induced a low level of other alternatively spliced products. **(C)** Quantification of correctly spliced exons (full-length) from *NLRP3* mRNA relative to the predominant ASO-mediated isoforms. Data are presented as mean ± SEM, unpaired t-test compared to matched control, *P<0.05, **P<0.01, ***P<0.001, ****P<0.0001; n=3.

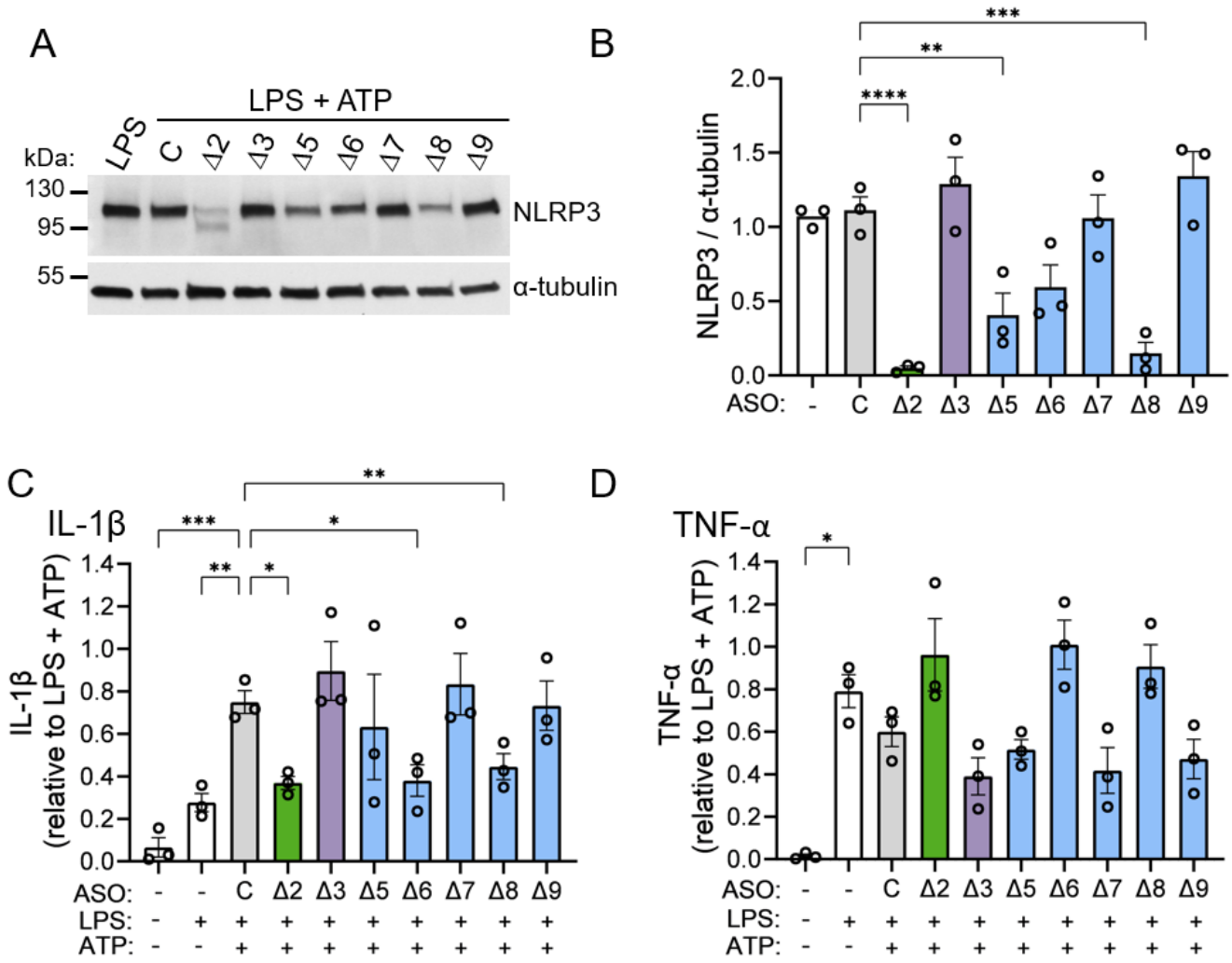


**Figure 2. ASO-induced *NLRP3* exon skipping inhibits inflammasome activation in human THP-1 cells.**

**(A)** Representative immunoblot of NLRP3 in THP-1 lysates treated with indicated ASOs (40 μM) followed by activation with LPS (100 ng/mL, 3 hr) and ATP (5 mM, 1 hr). α-tubulin was analyzed as a control. **(B)** Quantification of immunoblots of NLRP3 shown relative to α-tubulin control (mean ± SEM; n=3; **P<0.01, ***P<0.001, ****P<0.0001, ordinary one-way ANOVA with Dunnett's multiple comparisons test relative to ASO-C). ELISA analysis of **(C)** IL-1β and **(D)** TNF-α secreted from THP-1 cells treated with ASOs for 48 hours before activation with LPS and ATP. Cytokines were normalized to LPS and ATP stimulated cells. Data are presented as mean ± SEM and analyzed by repeated measures one-way ANOVA followed by Dunnett's multiple comparisons test relative to ASO-C or LPS only, respectively; *P<0.05, **P<0.01, ***P<0.001, ****P<0.0001. At least 3 independent experiments.

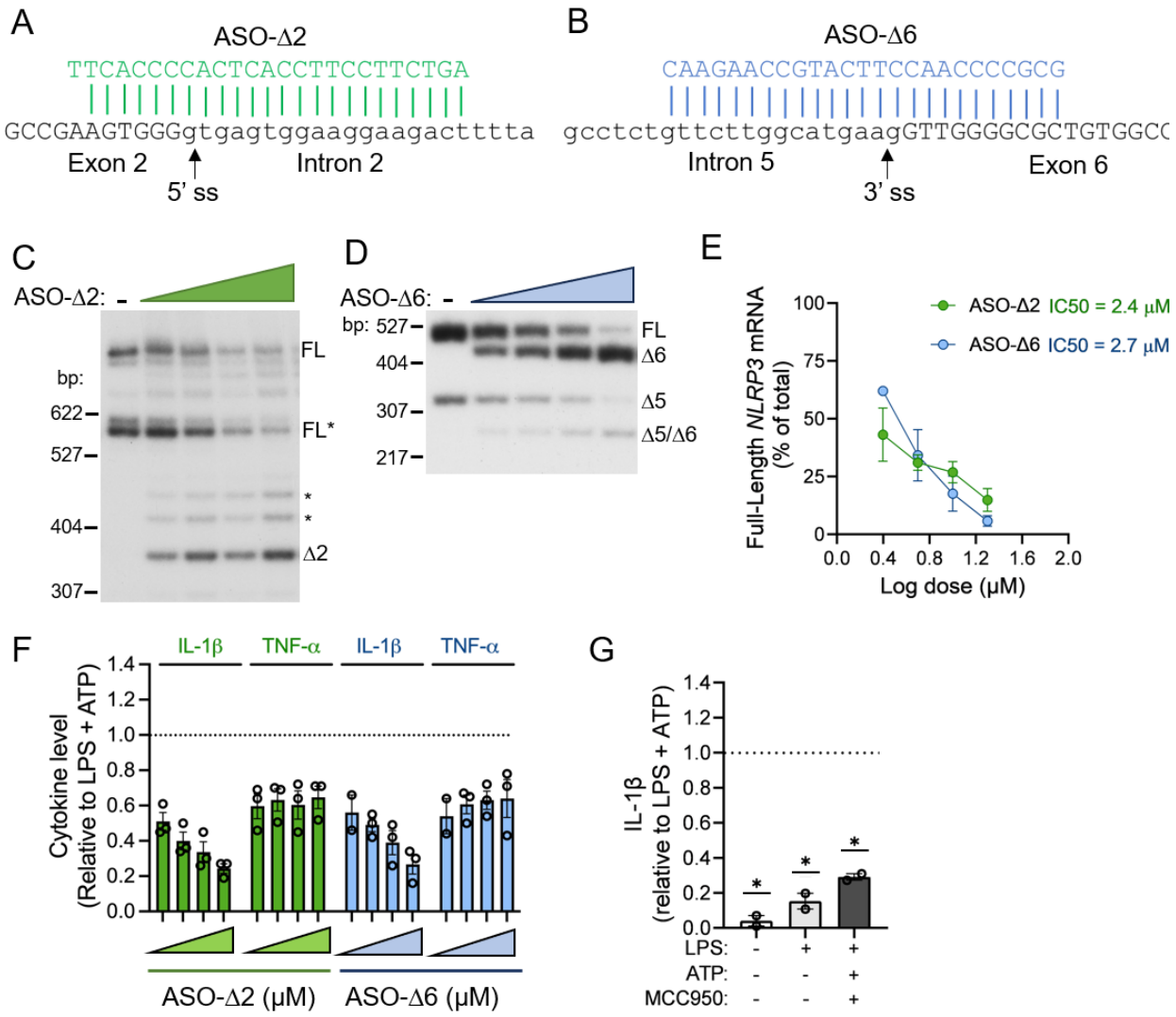


**Figure 3. *NLRP3*-targeted ASOs induce exon skipping in a dose-dependent manner in THP-1 cells.** **(A)** Sequence alignment of ASO-Δ2 base-pairing target sequence at the *NLRP3* exon 2 (capital letters)/intron 2 (lowercase) junction. 5' splice site (ss) of exon 2 is shown with arrow. **(B)** Sequence alignment of ASO-Δ6 base-pairing target sequence at the *NLRP3* intron 5 (lowercase)/exon 6 (capital letters) junction. 3' splice site (ss) of exon 6 is shown with arrow. **(C)** Representative radioactive RT-PCR analysis of *NLRP3* isoform expression in THP-1 cells transfected with increasing doses of ASO-Δ2 (2.5 μM-20 μM) for 48 hr. FL* denotes a naturally occurring full-length isoform. Other potential spliced products marked with asterisk (*). Products were amplified using a forward primer targeting exon 1 and a reverse primer targeting exon 4 and separated by PAGE. A non-targeted ASO was used as a control. **(D)** Representative radioactive RT-PCR analysis of *NLRP3* isoform expression in THP-1 cells transfected with increasing doses of ASO-Δ6 (2.5 μM-20 μM) for 48 hr. Products were amplified using a forward primer targeting exon 4 and a reverse primer targeting exon 7 and separated by PAGE. A non-targeted ASO was used as a control. **(E)** Quantification of correctly spliced exons (full-length) from *NLRP3* mRNA relative to the predominant ASO-mediated isoforms. ASO potency was calculated using the half maximal inhibitory concentration (IC50) after plotting the data on a nonlinear regression curve with a standard slope; ASO-Δ2 n=3; ASO-Δ6 n=2. ELISA analysis of **(F)** IL-1β and TNF-α secreted from THP-1 cells transfected with increasing doses of ASO-Δ2 (2.5 μM-20 μM) or ASO-Δ6 (2.5 μM-20 μM) and activated with LPS (100 ng/mL, 3 hr) and ATP (5mM, 1 hr). Cytokines were normalized to LPS and ATP stimulated cells (represented by a dotted horizontal line). At least 3 independent experiments. **(G)** ELISA analysis of IL-1β secreted from THP-1 cells treated with LPS (100 ng/mL, 3 hr), MCC950 (100 nM, 30 min) and ATP (5 mM) ± MCC950 (100 nM) for 1 hr. Data are presented as mean ± SEM and analyzed by one sample t-test relative to LPS and ATP (represented by dotted line); *P<0.05; n=2. At least 2 independent experiments.

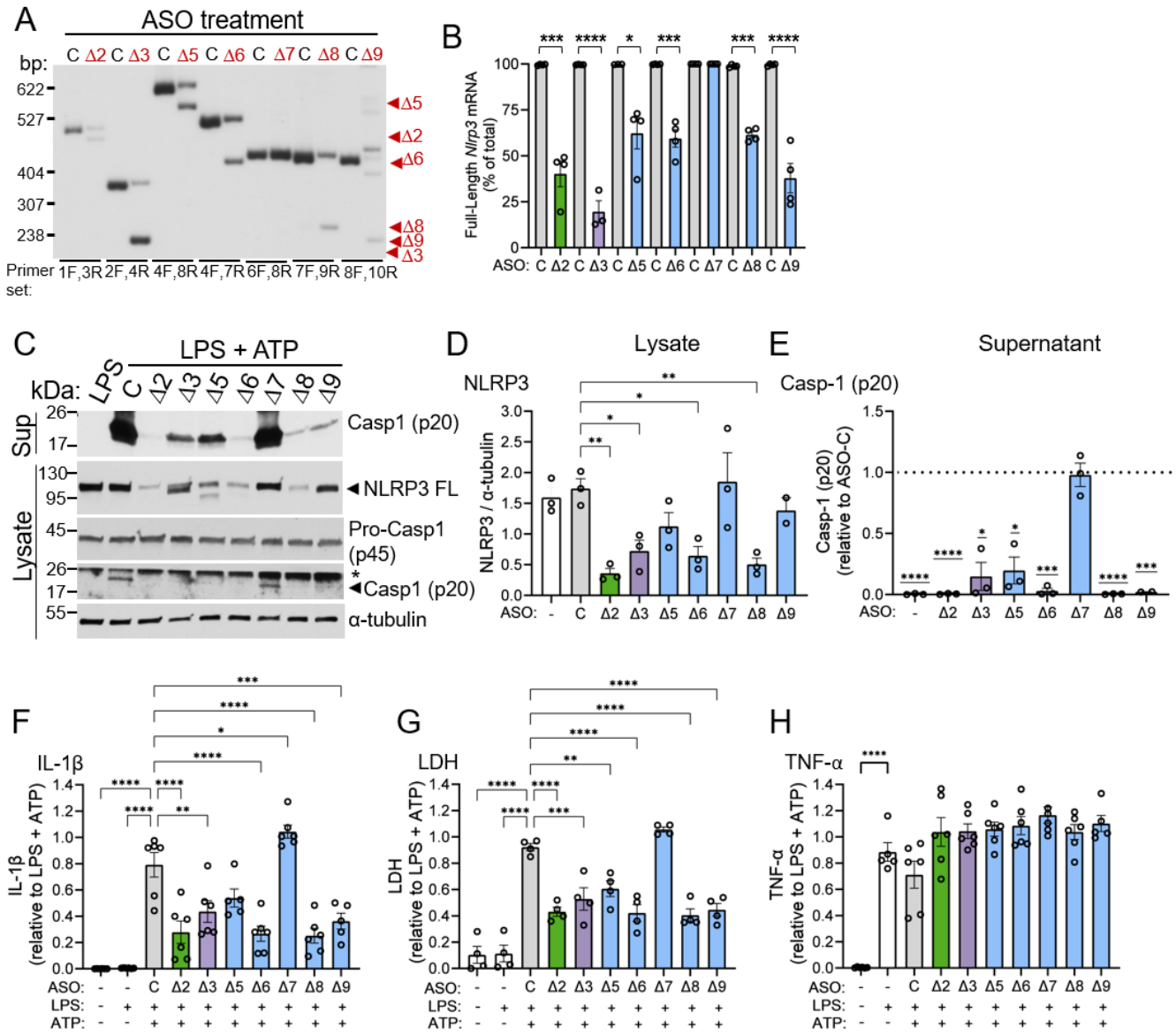


**Figure 4. ASO-mediated *Nlrp3* exon skipping reduces inflammasome signaling in mouse iBMDM.** **(A)** Representative radioactive RT-PCR analysis of *Nlrp3* RNA expression in iBMDMs transfected with indicated ASOs (40 μM) followed by activation with LPS (100 ng/mL, 3 hr) and ATP (5 mM, 1 hr). Products were amplified using different primer sets for each exon and separated by PAGE. A non-targeted ASO was used as a control (C). Red arrowheads indicate ASO-induced spliced products for each targeted exon. **(B)** Quantification of correctly spliced exons (full-length) from *Nlrp3* mRNA relative to the predominant ASO-mediated isoform. Data are presented as mean ± SEM, unpaired t-test compared to matched control, *P<0.05, **P<0.01, ***P<0.001, ****P<0.0001; n=4. **(C)** Representative immunoblot of NLRP3, Pro-Casp1 and cleaved Casp1 (p20) in iBMDM lysates and Casp1 (p20) in iBMDM supernatant treated with indicated ASOs (40 μM) followed by activation with LPS and ATP. α-tubulin was analyzed as a control. Asterisks denote non-specific bands. **(D)** Quantification of immunoblots of NLRP3 shown relative to α-tubulin control (mean ± SEM; n=3; **P<0.01, ***P<0.001, ****P<0.0001, one-way ANOVA with Dunnett's multiple comparisons test relative to ASO-C). **(E)** Quantification of immunoblots of cleaved Casp1 (p20) secretion from iBMDM treated with ASOs for 48 hours before activation with LPS and ATP. Casp1 (p20) relative to ASO-C (mean ± SEM; n=3; **P<0.01, ***P<0.001, ****P<0.0001, one sample t-test compared to 1). ELISA analysis of **(F)** IL-1β, **(G)** LDH and **(H)** TNF-α secreted from iBMDMs treated with ASOs for 48 hours before activation with LPS and ATP. Cytokines were normalized to LPS and ATP stimulated cells. Data are presented as mean ± SEM and analyzed by ordinary one-way ANOVA followed by Dunnett's multiple comparisons test relative to ASO-C or LPS only, respectively; LDH n=4; *P<0.05, **P<0.01, ***P<0.001, ****P<0.0001. At least 3 independent experiments.

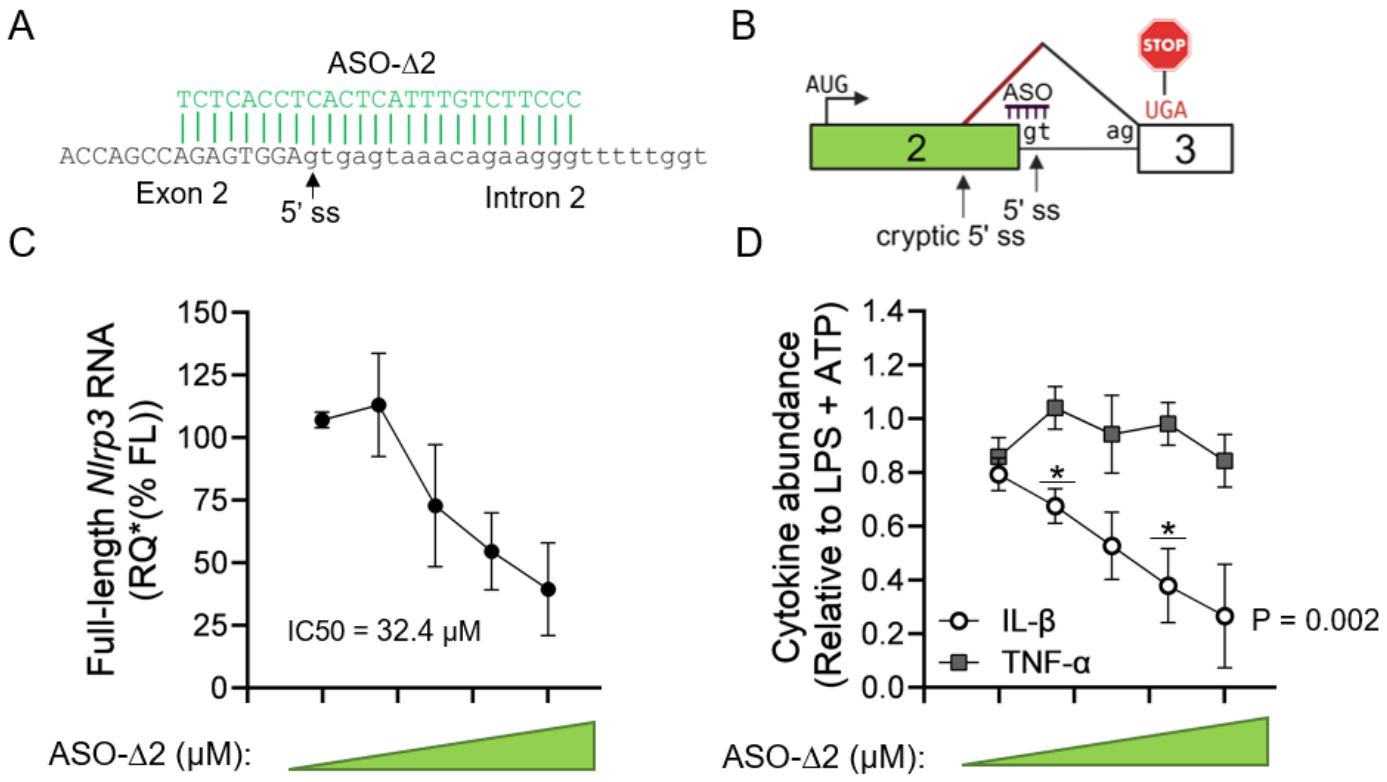


**Figure 5. ASO-Δ2 dose-dependent modulation of *Nlrp3* exon 2 splicing in mouse iBMDM.** **(A)** Sequence alignment of ASO-Δ2 base-pairing target sequence at the *Nlrp3* exon 2 (capital letters)/intron 2 (lowercase) junction. 5' splice site (ss) of exon 2 is shown with arrow. **(B)** ASO-Δ2 mechanism of action illustrating the activation of a cryptic 5' ss in exon 2 that shifts the open reading frame and results in a premature termination codon in exon 3. Boxes are exons and lines are introns. General ASO base-pairing site is labeled. Diagonal black line shows splicing of introns. Red diagonal line indicates ASO-induced splicing event. AUG indicates a start codon and UGA indicates a termination codon. **(C)** Quantification of correctly spliced exons (full-length) from *Nlrp3* mRNA relative to the predominant ASO-mediated isoform in iBMDM cells transfected with increasing doses of ASO-Δ2 (2.5 μM-40 μM) for 48 hr. Percent full-length (% FL) was multiplied by the relative quantity (RQ) of *Nlrp3* mRNA remaining to correct for degraded RNA. ELISA analysis of **(D)** IL-1β and TNF-α secreted from iBMDM cells transfected with increasing doses of ASO-Δ2 and activated with LPS (100 ng/mL, 3 hr) and ATP (5 mM, 1 hr). Cytokines were normalized to LPS and ATP stimulated cells. Individual data points are presented as mean ± SEM and analyzed by one sample t-test compared to LPS and ATP set to 1; *P<0.05; n=3. The slope of the dose response curve was analyzed by simple linear regression (P=0.002). At least 3 independent experiments.

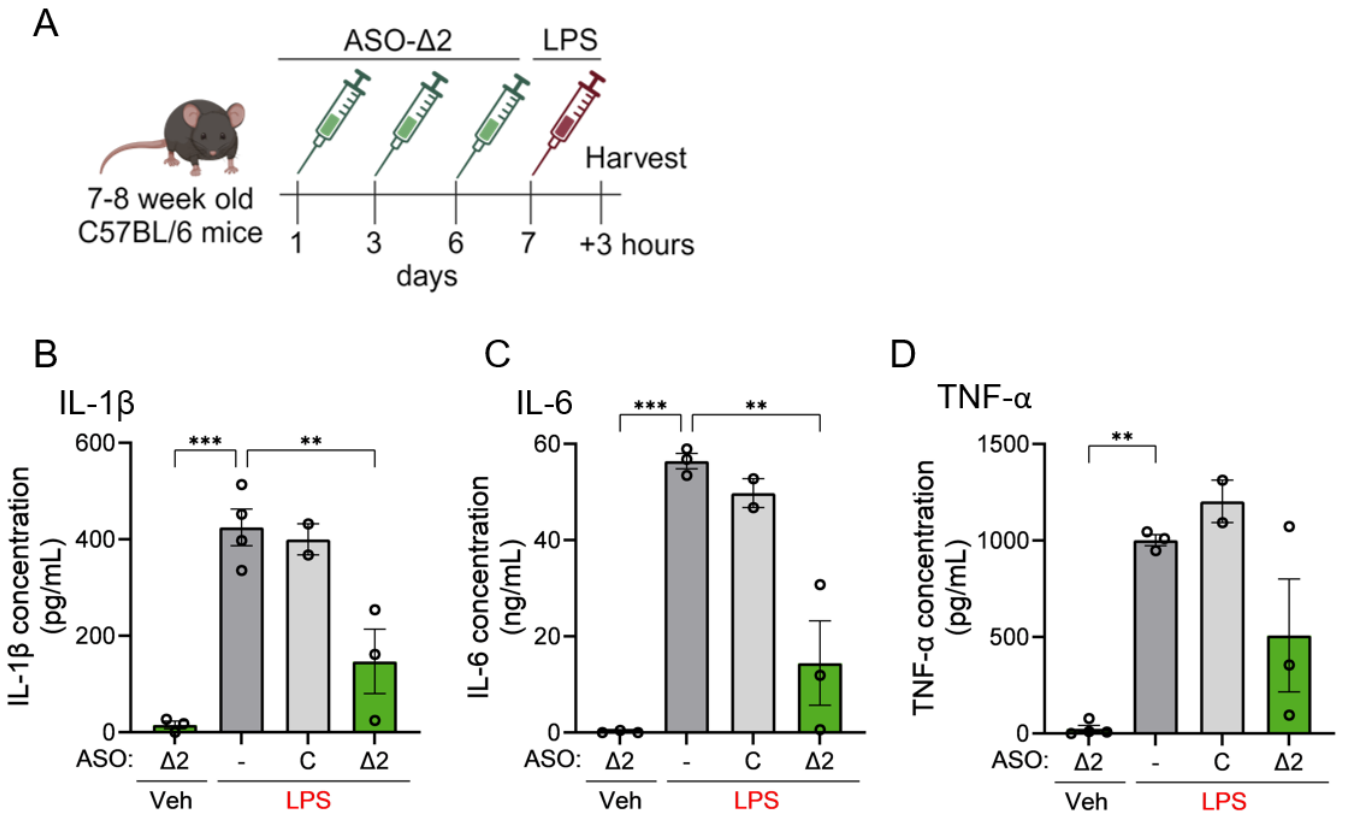


**Figure 6. ASO-mediated *Nlrp3* exon 2 skipping reduces systemic inflammation *in vivo*.**
**(A)** Schematic of dosing regimen in 7-8 week-old mice. Mice were treated three times with either ASO-Δ2 (100 mg/kg; n=3), PBS vehicle (n=3-4) or non-targeted control ASO (100 mg/kg; n=2) followed by treatment with either LPS or PBS vehicle. ELISA analysis of **(B)** IL-1β, **(C)** IL-6, and **(D)** TNF-α in the plasma. Symbols represent individual mice. Data are presented as mean ± SEM; *P<0.05, **P<0.01, ***P<0.001. Ordinary one-way ANOVA followed by Dunnett's multiple comparisons test relative to PBS control.

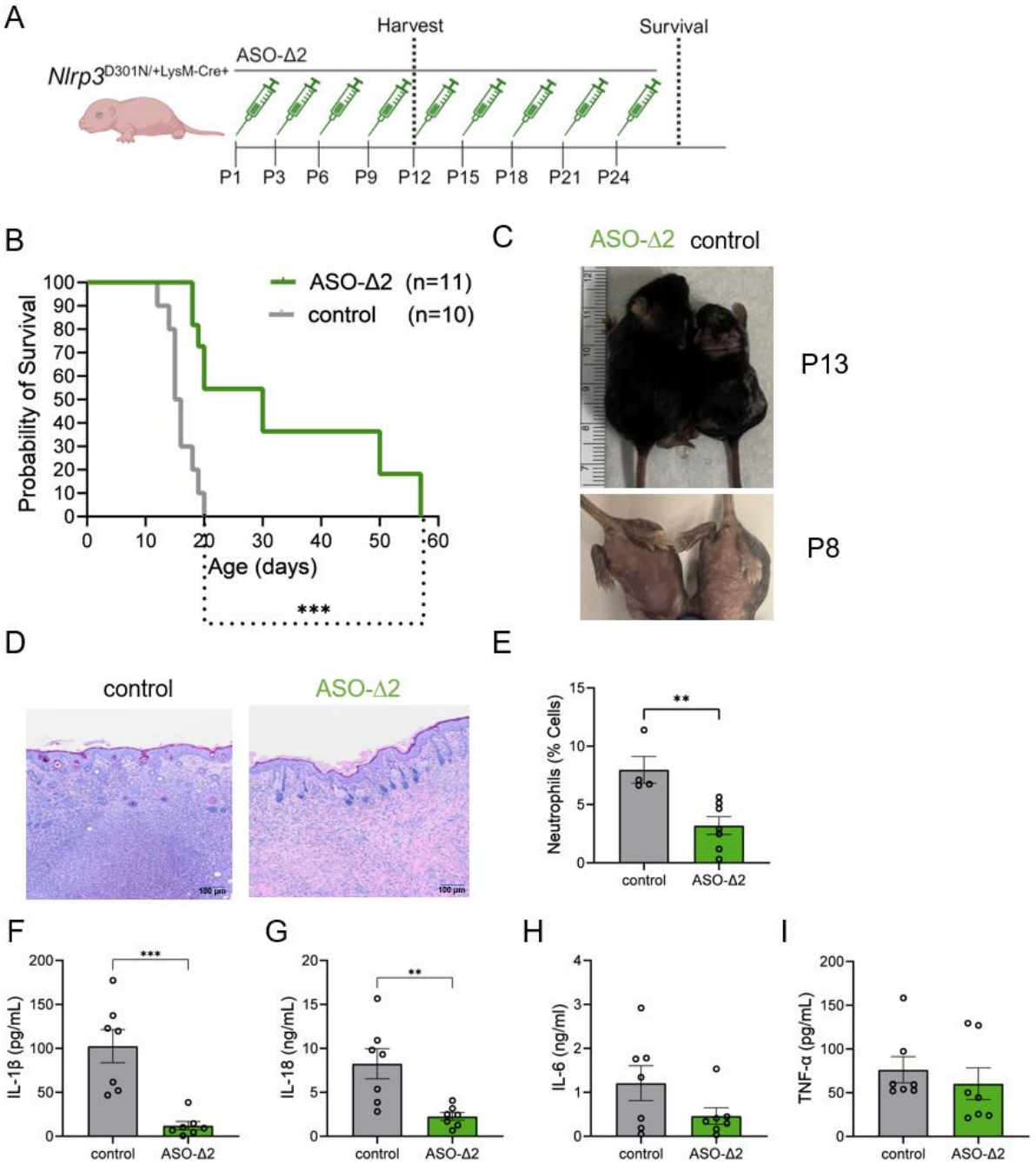


**Figure 7. ASO-Δ2 prolongs survival and alleviates systemic inflammation in CAPS mice.**
**(A)** Schematic of dosing regimen in Nlrp3$^{D301N/+\ LysMCre+}$ CAPS neonates. Control littermates were injected with PBS vehicle. **(B)** Kaplan–Meier survival curve. Curve comparison for ASO-Δ2 (n=11) vs. PBS control (n=10), P=0.0003, Gehan-Breslow-Wilcoxon test. **(C)** Images of representative ASO and control-treated Nlrp3$^{D301N/+\ LysMCre+}$ mice. **(D)** Representative images of H&E staining of skin of ASO-treated mice (n=7) compared to controls (n=4). Scale bars, 100 μm. **(E)** Quantification of neutrophil infiltration of skin from ASO-treated mice (n=7) compared to controls (n=4). ELISA analysis of **(F)** IL-1β, **(G)** IL-18, **(H)** IL-6, and **(I)** TNF-α in the serum of ASO-Δ2 or control treated CAPS pups collected at P12 (n=7 per group). Data are mean ± SEM, unpaired t-test *P<0.05, **P<0.01, ***P<0.001. P, postnatal day.

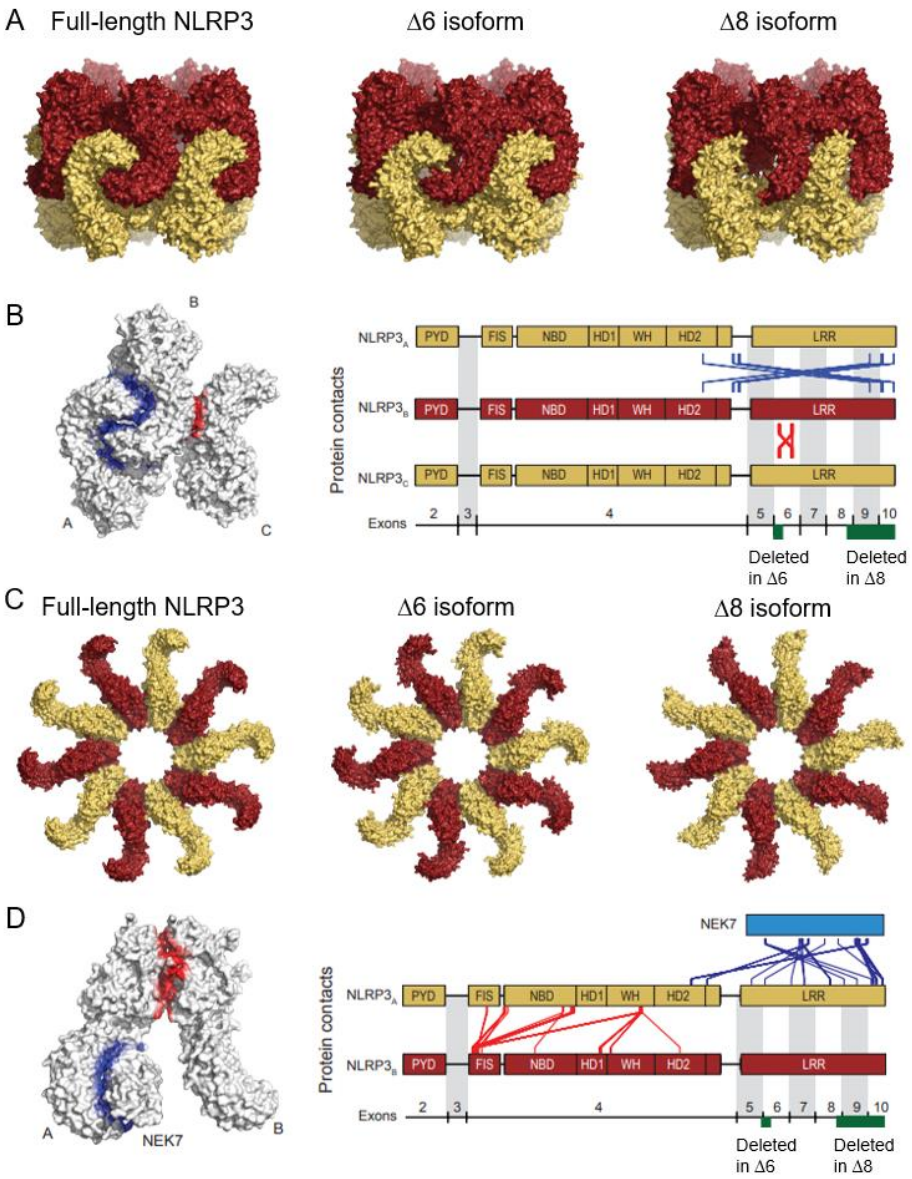


**Supplemental Figure 1. Structural modeling of the Δ6 and Δ8 NLRP3 isoforms.** The Δ6 and Δ8 NLRP3 isoforms are predicted to affect the stability of the inactive decamer cage assembly and potentially the NLRP3-NEK7 interaction in the active disk assembly. **(A)** Comparison of the inactive decameric cage form of full-length NLRP3 (left, PDB id 7pzc; (22)) and Alphafold2 models of the Δ6 and Δ8 isoforms superimposed onto the full-length structure. **(B)** Depiction of the two unique interaction surfaces of the decameric NLRP3 cage assembly between the concave (blue) and convex (red) faces of the LRR domains (left). Mapping of the interactions onto a linear diagram of the NLRP3 proteins reveals that the Δ6 isoform specifically deletes a region of the LRR involved in the convex interaction (indicated green box) and that the Δ8 isoform deletes most of the regions making up the concave interactions (indicated green box). Both isoforms, but particularly the Δ8 isoform, would be predicted to disrupt the stability of the decameric cage. In the case of the Δ6 isoform, changes due to the deletion could both weaken the convex interactions as well as alter the concave interactions by changing the spacing of the LRR repeats C-terminal to the deletion. **(C)** Comparison of the active disk form of full-length NLRP3 (left, PDB id 8ej4; (42)) and Alphafold2 models of the Δ6 and Δ8 isoforms superimposed onto the full-length structure. **(D)** Depiction of the two unique interaction surfaces of the active decameric NLRP3 disk assembly between adjacent NLRP3 monomers (red) and NEK7 (blue) (left). Mapping of the interactions onto a linear diagram of the NLRP3 proteins suggests that both LRR deletions are unlikely to affect the decameric disk formation, as these interactions are mediated by the FIS and NACHT domains that are not affected in the Δ6 and Δ8 isoforms. In contrast, the Δ8 isoform eliminates many of the residues involved in the full-length LRR-NEK7 interaction (indicated green box), suggesting a weaken interaction.

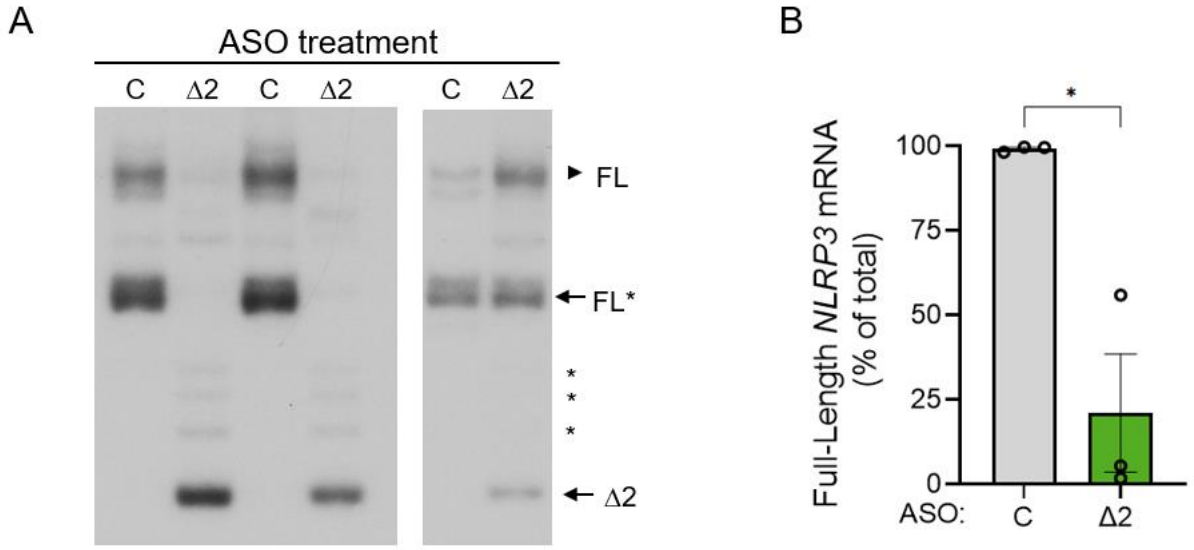


**Supplemental Figure 2. ASO-Δ2 modulates *NLRP3* exon skipping in human monocyte-derived macrophages (hMDM) from persons with CAPS. (A)** Representative radioactive RT-PCR analysis of *NLRP3* isoform expression in *NLRP3*$^{L353P/+}$ hMDM cells transfected with ASO-Δ2 (40 μM) for 24 hr. Other potential spliced products marked with an asterisk (*). FL* denotes a naturally occurring full-length isoform. Products were amplified using a forward primer targeting exon 1 and a reverse primer targeting exon 4 and separated by PAGE. A non-targeted ASO was used as a control. **(B)** Quantification of correctly spliced exons (full-length) from *NLRP3* mRNA relative to the predominant ASO-mediated isoforms. Data are presented as mean ± SEM, unpaired t-test compared to matched control, *P<0.05; N=3 patients.

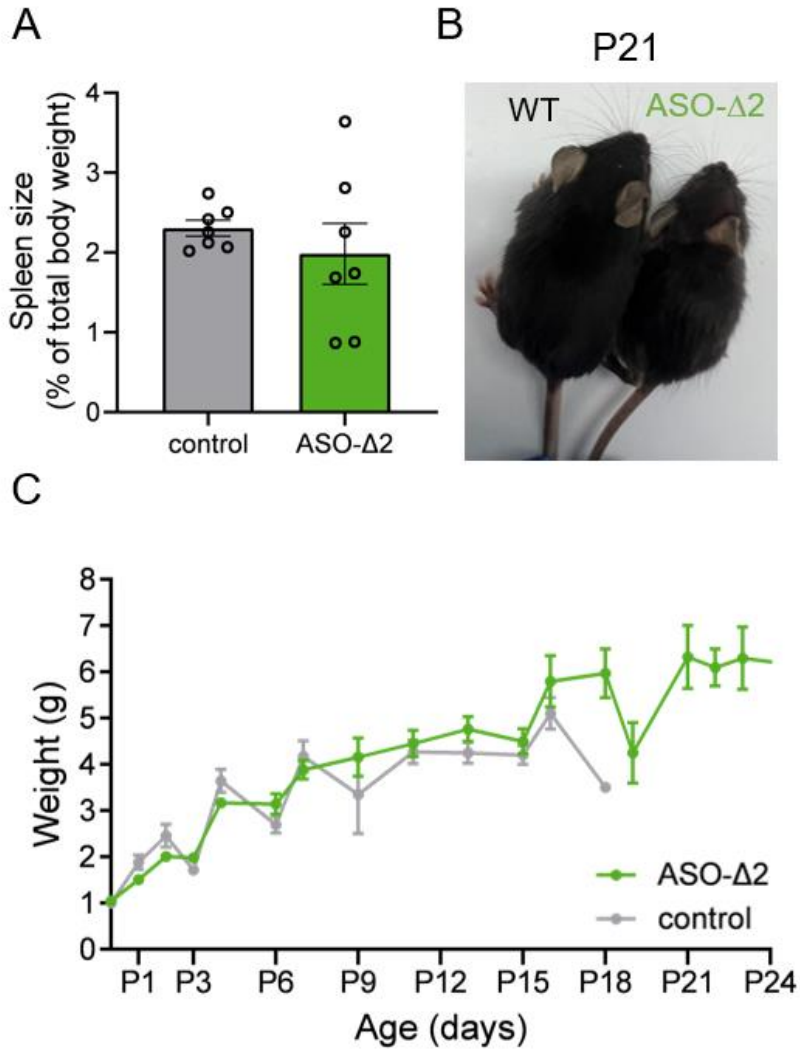


**Supplemental Figure 3. Weight and spleen size of ASO-treated CAPS mice. (A)** Spleen size relative to total body weight at day 12 (n=7 per group). **(B)** Representative image of ASO-treated Nlrp3$^{D301N/+\ LysMCre+}$ and wild type (WT) mice at P21. **(C)** Growth curve of ASO and control treated Nlrp3$^{D301N/+\ LysMCre+}$ pups.

**Supplementary Table 1. Splice-switching Antisense Oligonucleotides and Primers**

| Primer | Sequence (5'-3') |
|---|---|
| hNLRP3ex1F | TTCCTGAGGCTGGCATCT |
| hNLRP3ex4R | TCTTGGTCTTGCCGATGGC |
| hNLRP3ex2F | CCGAGGGGTCAGACAGAGAA |
| hNLRP3ex4F | AGGCCGACACCTTGATA |
| hNLRP3ex7R | CCCAGTTTCTGCAGGTTAC |
| hNLRP3ex6F | CAGAAGCTGGTGGAGCTG |
| hNLRP3ex8R | GAGAGTGTTGCCTCGCAG |
| hNLRP3ex7F | CATTCCCTGACCAGACTCT |
| hNLRP3ex9R | CTCTGCTGTTTCAGCACTTC |
| hNLRP3ex8F | GTTGGTGAATTCTGGCCTTAC |
| hNLRP3ex10R | GAAGTGTTTCTAACGCAC |
| mNlrp3ex1F | TGGTCAGACACGAGTCCTG |
| mNlrp3ex3R | TGGTATGCCAGGAGGACA |
| mNlrp3ex2F | TGCGATCAACAGGCGAGAC |
| mNlrp3ex4R | AGCATGAACTCCTGACCATCGG |
| mNlrp3ex4F | GAGATCAACCTCTCTACCAG |
| mNlrp3ex7R | GATGTGAGACAGCAGCTC |
| mNlrp3ex6F | ATCAATGCTGCTTCGACATC |
| mNlrp3ex8R | GTAGATAGAGGTGTGTGAAG |
| mNlrp3ex7F | ATTGGTTCTGAGCTCCAACC |
| mNlrp3ex9R | CGCCAAGATCATTGTTGCCCAG |
| mNlrp3ex8F | TCCGGCCTTACTTCAATCTG |
| mNlrp3ex10R | TGGAGCGCTTCTAAGGCAC |
| **Oligo** | **Sequence (5'-3')** |
| human NLRP3-201 e2i2 | AGTCTTCCTTCCACTCACCCCACTT |
| human NLRP3-201 e3i3 | GAAGCACCACCCCAGTCGCTTACCT |
| human NLRP3-201 e5i5 | TTCACCAATCTAGGAATTAGAAGGA |
| human NLRP3-201 i5e6 | GCGCCCCAACCTTCATGCCAAGAAC |
| human NLRP3-201 e7i7 | ACACCCATGAAGACTTACCCCAGTT |
| human NLRP3-201 e8i8 | AACCAAAGGACTTACTCCAACACCT |
| human NLRP3-201 e9i9 | TGCAGAGCACACTCACCCCAGGTTC |
| mouse Nlrp3-202 e2i2 | CCCTTCTGTTTACTCACTCCACTCT |
| mouse Nlrp3-202 e3i3 | GCAGAAGCTTGACGCTTACCTTTCT |
| mouse Nlrp3-202 e5i5 | CACACACAGACTTACCACAGTCTCT |
| mouse Nlrp3-202 e6i6 | AGGTAGGCCAGACTCACCACAGTTT |
| mouse Nlrp3-202 i6e7 | GCTCACCAACCTTCCATGCAGAGGG |
| mouse Nlrp3-202 e8i8 | GGCAGCCCATGAACTCACTCCAGCA |
| mouse Nlrp3-202 e9i9 | AGGCAAACCACACTCACTGTAGGCT |
| Non-targeted control | CCTCTTACCTCAGTTACAATTTATA |